buildings

MDPI

Article

Attachment and Visual Observation of a Photonic Crystal-Based Mechanochromic Sensor on Concrete, Masonry, and Timber Components: A Preliminary Experimental Evaluation

Kyong-Chul Kim [1], Youngmin Kim [2], Gum-Sung Ryu [1] and Changhyuk Kim [2,*]

[1] Department of Structural Engineering Research, Korea Institute of Civil Engineering and Building Technology, Goyang-si 10223, Republic of Korea; kim6069@kict.re.kr (K.-C.K.); ryu0505@kict.re.kr (G.-S.R.)
[2] Department of Architectural Engineering, Inha University, Incheon 22212, Republic of Korea; appleyoung98@inha.edu
* Correspondence: changhyuk@inha.ac.kr; Tel.: +82-32-860-7565

Abstract

Crack monitoring in building components requires sensing methods that accommodate different surface conditions while maintaining consistent observation conditions. This preliminary study investigated a photonic crystal-based mechanochromic sensor for visual crack monitoring of concrete, masonry, and timber components. Attachment and observation characteristics were examined considering surface conditions and crack behavior. In the concrete T girder, the sensor tended to change from blue toward green hues as cracking progressed and detached at the shear failure stage. For masonry, the attachment location and method were selected considering surface irregularities between bricks and mortar joints, and crack development was observed with a crack gauge installed near the sensor. For timber, irregular crack paths and difficulties in direct attachment were observed, and a clamping frame was applied to restrain displacement and rotation of the sensor. A measurement device was developed to maintain the relative positions of the sensor, camera, and light source during repeated imaging. Based on these observations, attachment and image-acquisition procedures were proposed for repeated visual crack monitoring. Initial remote image-acquisition functions were implemented, and an integrated architecture incorporating Long-Term Evolution (LTE) and an independent power supply was proposed to support future expansion to practical applications.

Keywords: mechanochromic sensor; structural health monitoring; structural members; photonic crystal; optical measurement; crack monitoring; deformation transfer

Check for updates

Academic Editor: Antonio Caggiano

Received: 21 September 2026
Revised: 15 October 2026
Accepted: 22 October 2026
Published: 24 October 2026

Copyright: © 2026 by the authors. Licensee MDPI, Basel, Switzerland. This article is an open access article distributed under the terms and conditions of the Creative Commons Attribution (CC BY) license.

1. Introduction

Cracks in structural components may develop due to material volume changes, deformation under external loads, and long-term deterioration. In reinforced concrete, these cracks can facilitate the penetration of chlorides, moisture, and oxygen, thereby accelerating reinforcement corrosion and reducing durability. Poursaee and Ross [1] reported general agreement that cracks affect the initiation of rebar corrosion. However, the influence of cracks and crack width on long-term corrosion propagation remains under debate and may vary with exposure conditions, cover depth, crack spacing, and crack orientation. Accordingly, effective maintenance of structures requires not only the detection of cracks but also repeated monitoring of their progression at the same locations.

Various measurement technologies, including strain gauges, displacement transducers, capacitive sensors, and fiber optic sensors, have been applied to monitor cracks and associated deformation in structural members. Yan et al. [2] applied a sensing skin comprising an array of flexible capacitive sensors to reinforced concrete and post-tensioned concrete beams and demonstrated its capability for crack detection, localization, and quantification. Distributed fiber optic sensing can capture strain distributions around cracks. However, interpretation of the measured response requires consideration of strain transfer from the member to the optical fiber at displacement discontinuities. Bassil et al. [3] proposed a strain transfer model considering imperfect bonding at multilayer interfaces. Zhang et al. [4] developed a mechanical model to interpret fiber strain responses at displacement discontinuities and validated the model through cable calibration and concrete cracking tests. These studies indicate that crack-induced sensor responses are affected by strain transfer from the structural member to the sensor through the bonding layers.

Image-based methods enable non-contact monitoring of surface cracks and deformation in structural components. Hoult et al. [5] proposed a digital image correlation (DIC) method to measure crack width and slip in reinforced concrete. Cha et al. [6] developed a convolutional neural network (CNN)-based method for detecting concrete cracks. Belloni et al. [7] combined photogrammetry and deep learning to monitor crack changes using images acquired from different camera positions. Omoniyi et al. [8] examined data augmentation for custom and pre-trained CNN crack-detection models, and Ribeiro et al. [9] reviewed remote bridge-inspection methodologies. Crack detection and displacement measurement require different image information. Their performance can also be affected by imaging conditions and changes in the camera geometry.

A mechanochromic sensor converts mechanical deformation into a visible color change and can be used to monitor cracks in structural components. Bae et al. [10] attached a thin-film mechanochromic sensor to a metal specimen and quantified the deformation by analyzing the RGB components of images captured with a smartphone. They also developed a Fabry–Perot mechanochromic sensor with reduced viewing-angle dependence using a metal–dielectric–metal resonator [11]. Pyeon et al. [12] investigated the effects of concrete surface finishing conditions on the deformation and color response of a mechanochromic sensor. In a subsequent study, Pyeon et al. [13] examined sensor color changes associated with cracking in cementitious specimens and concrete beam members and evaluated the recovery of the color response after freeze–thaw exposure. Numerous studies have demonstrated the applicability of mechanochromic sensors to deformation measurement and crack monitoring. However, studies that sufficiently consider surface conditions, crack propagation, sensor attachment, and observation conditions for application to structural components remain limited.

Photonic crystal-based sensors use structural-color changes caused by variations in the spacing of periodic microstructures under mechanical deformation. Minh et al. [14] developed a photonic crystal strain sensor on a flexible polydimethylsiloxane (PDMS) substrate and proposed a method to compensate for viewing angle effects. Quan et al. [15] used diffractive structural colors to measure tensile, biaxial, and shear deformation. Hoang Minh et al. [16] fabricated strain-sensitive and strain-insensitive photonic crystals on the same substrate to compensate for viewing angle effects. The proposed devices were applied as strain sensors and chemical indicators. Battisti et al. [17] quantified mechanochromic color changes in polymer systems using hue values in the hue, saturation, and value (HSV) color space. Kang et al. [18] evaluated the mechanical stability of an infrared emitter formed on a flexible substrate. The emitter showed no delamination after bending to a radius of curvature of 0.5 cm and no appreciable change in emissivity after 100 bending cycles at a radius of curvature of 1.0 cm. However, these studies mainly evaluated the optical

and mechanical responses of fabricated devices or specimens under controlled laboratory conditions. Studies that sufficiently consider the surface conditions and crack behavior of structural components together with sensor attachment and observation characteristics remain limited. Sensor flexibility, surface irregularities, and local surface changes during crack propagation can affect the attachment condition. Therefore, the attachment method should maintain stable attachment to the member while allowing crack-induced deformation to be transferred to the sensor.

Choi et al. [19] analyzed color changes in a photonic crystal-based sensor under uniaxial displacement using the RGB and HSV color spaces and applied the results to image-based displacement prediction. The dominant color component varied with the displacement level under controlled light and image conditions. However, crack opening and tangential slip can occur simultaneously in structural components. Crack propagation can also change the attachment surface and affect deformation transfer to the sensor. In addition, sensor rotation can change the relative positions of the sensor, camera, and light source. Therefore, studies that sufficiently consider sensor attachment, observation conditions, and crack-induced deformation transfer for crack measurement in structural components remain limited.

In this study, a photonic crystal-based mechanochromic sensor was applied to concrete, masonry, and timber components to examine attachment and observation characteristics under different surface conditions and crack behaviors. Sensor color changes associated with crack development were also observed in concrete and timber. This study examined material-specific sensor attachment and observation characteristics, including attachment and detachment in concrete, installation around uneven masonry joints, and sensor-positioning using a frame and irregular crack paths in timber. These case observations inform proposed installation and image-acquisition considerations for the three materials. Sensor attachment and color changes were examined using images and observations obtained during installation and test. The factors affecting deformation transfer and continued observation were also examined. A measurement device was developed to maintain the relative positions of the sensor, camera, and light source. Installation and measurement procedures were proposed for sensor placement, recording of the initial condition, and repeated observation. In addition, a remote image monitoring system using solar power and wireless communication was proposed for environments where continuous external power supply is limited.

2. Materials and Methods

2.1. Study Scope and Evaluation

Table 1 compares the scope of the previous study on color space analysis and displacement prediction with that of this study. This study focused on the application methodology of the sensor for monitoring cracks in structural components. The sensing principle and the relationship between uniaxial displacement and color under controlled conditions were adopted from previous studies [14,16,19]. Sensor attachment and observation characteristics were examined through tests on a concrete T girder, masonry walls, and a timber beam. Uniaxial tensile tests were additionally conducted on timber to examine the effects of grain direction and attachment method on sensor application.

The evaluation focused on sensor attachment, color changes associated with crack development, and changes in the bonded and unbonded areas. Observation conditions were examined separately in terms of image distance and view angle. Sensor attachment and crack development were examined for each material based on images obtained from the concrete girder, masonry walls, and timber specimens. For the concrete girder, images acquired at different load stages were used. For the masonry walls, installation and

crack development images were examined. Uniaxial tensile tests and beam tests were conducted on the timber specimens. Observed color changes and compromised attachment conditions were also examined. The evaluation is limited to qualitative observations of the documented cases; material-specific repeatability and statistical representativeness were not assessed.

Table 1. Comparison between the previous color-space and displacement-prediction study and the present study.

Category	Previous Study [19]	Current Study
Research question	Color response under uniaxial displacement	Sensor attachment and observation in structural components
Main target	Sensor mounted on a steel jig	Concrete, masonry, and timber components
Evaluation focus	RGB/HSV analysis and displacement prediction	Color change, attachment condition, and sensor visibility during cracking
Optical conditions	Fixed laboratory imaging conditions	Controlled observation geometry using a measurement device
Main outcome	Image-based displacement prediction	Application characteristics and monitoring procedure

2.2. Sensing Principle and Sensor Attachment

A photonic crystal-based mechanochromic sensor was used in this study. The sensor exhibits structural-color changes as the periodic nanostructure on the flexible substrate deforms. Previous studies [14,19] showed that the generated color is affected by the nanostructure period and the incident and viewing angles. Under fixed optical conditions, changes in the nanostructure period caused by axial strain result in a shift in the diffraction wavelength. The relationship between diffraction wavelength and sensor strain can be expressed as Equation (1) [14,19].

$$\frac{\lambda}{\lambda_0} = 1 + \varepsilon_s \quad (1)$$

where λ_0 and λ are the diffraction wavelengths before and after deformation, respectively, and ε_s is the sensor strain in the optically observed direction. Accordingly, attachment condition, deformation direction, and observation conditions were considered when applying the sensor to structural components.

Table 2 and Figure 1 summarize the sensor locations and attachment methods for each material. Both ends of the sensor were fixed to the component to transfer the relative displacement across the crack. The central part was left as a free sensing region that could deform without restraint from the adhesive. For the concrete component, the sensor was cut into a 10 × 30 mm rectangle. The attachment surface was ground and then cleaned with alcohol or acetone to remove dust, oil, and moisture. The bonding areas at both ends of the sensor were marked with tape, and a small amount of adhesive was applied only to these areas. The sensor ends were then fixed by applying uniform pressure. The amount of adhesive and sensor alignment were controlled to avoid adhesive intrusion into the free sensing region. The total sensor length was distinguished from the effective gauge length, L_g, defined as the freely deformable region between the two attachment regions.

For masonry, the sensor was placed across a mortar joint where cracking was expected. The attachment regions were located on the adjacent brick surfaces. Direct bonding to the mortar joint could reduce attachment stability because of the surface step and surface heterogeneity between the brick and mortar. Therefore, adhesive bonding to the brick surfaces was combined with mechanical clamping. For timber, both ends of the sensor were clamped to a light-shielding frame and positioned over the region where cracking was expected. Surface roughness and locally raised wood fibers were considered when

positioning the sensor. The frame was configured to restrain sensor displacement and rotation and to maintain a consistent observation position.

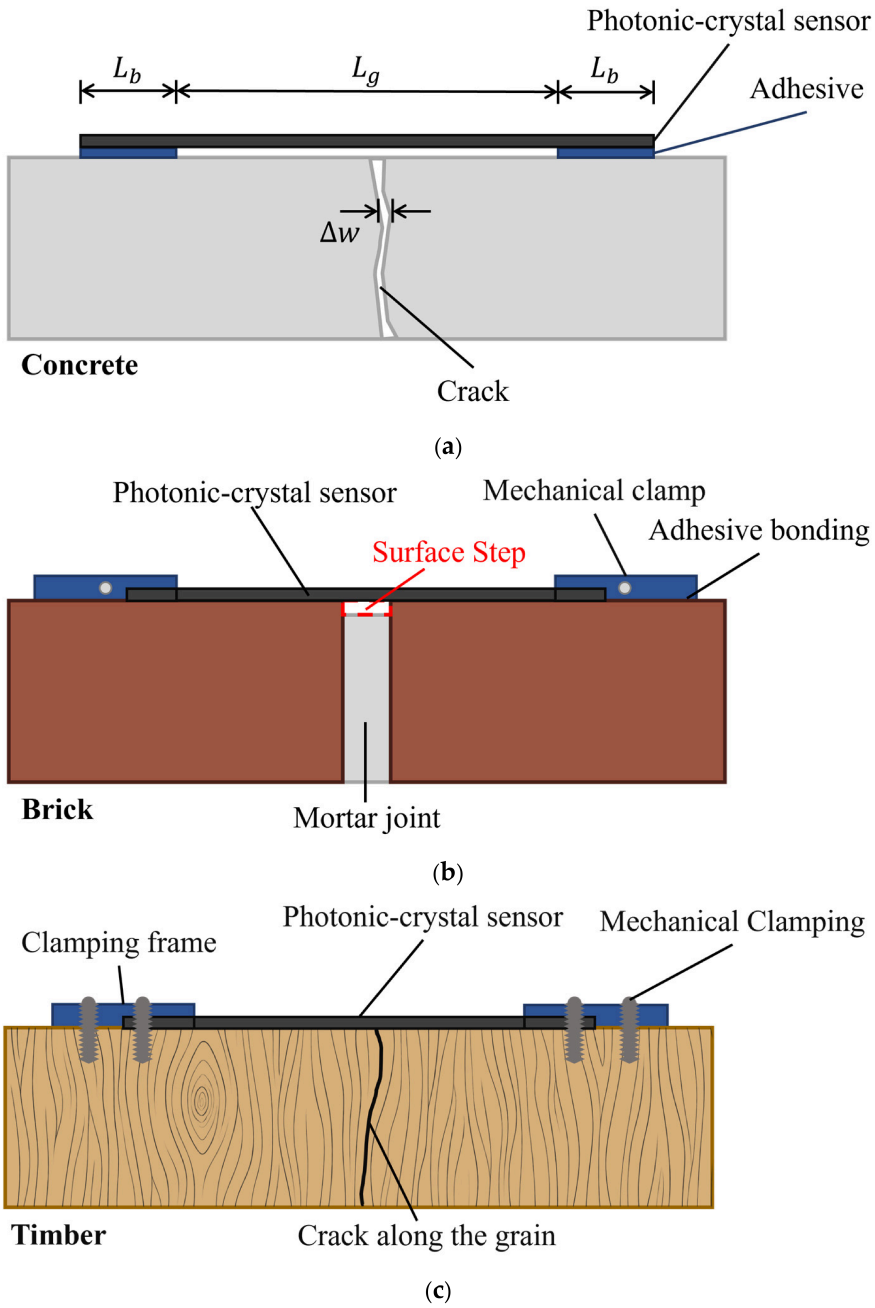


Figure 1. Schematic of sensor installation for each material. (**a**) Concrete: adhesive bonding at both ends and free sensing region; (**b**) masonry: attachment method accounting for the surface step at the mortar joint; (**c**) timber: frame-based clamping.

Table 2. Sensor placement and attachment methods for each material.

Material	Primary Placement Location	Attachment Method	Primary Control Item
Concrete	Existing or expected crack region	Adhesive bonding at both ends	Attachment stability and adhesive intrusion into the free sensing region
Masonry	Mortar joint and adjacent brick surfaces	Adhesive bonding with mechanical clamping	Surface step at the mortar joint and surface heterogeneity
Timber	Expected crack region	Clamping with a light-shielding frame	Crack direction, sensor rotation, and deformation transfer

2.3. Experimental Setup and Image Acquisition

Table 3 summarizes the geometry and observation targets of the main specimens, and Figure 2 shows the specimen configurations and measurement layout. A concrete T girder, masonry walls, and a timber beam were used to examine sensor application under different crack behaviors and surface conditions. The masonry walls consisted of two specimen types with different brick surface conditions.

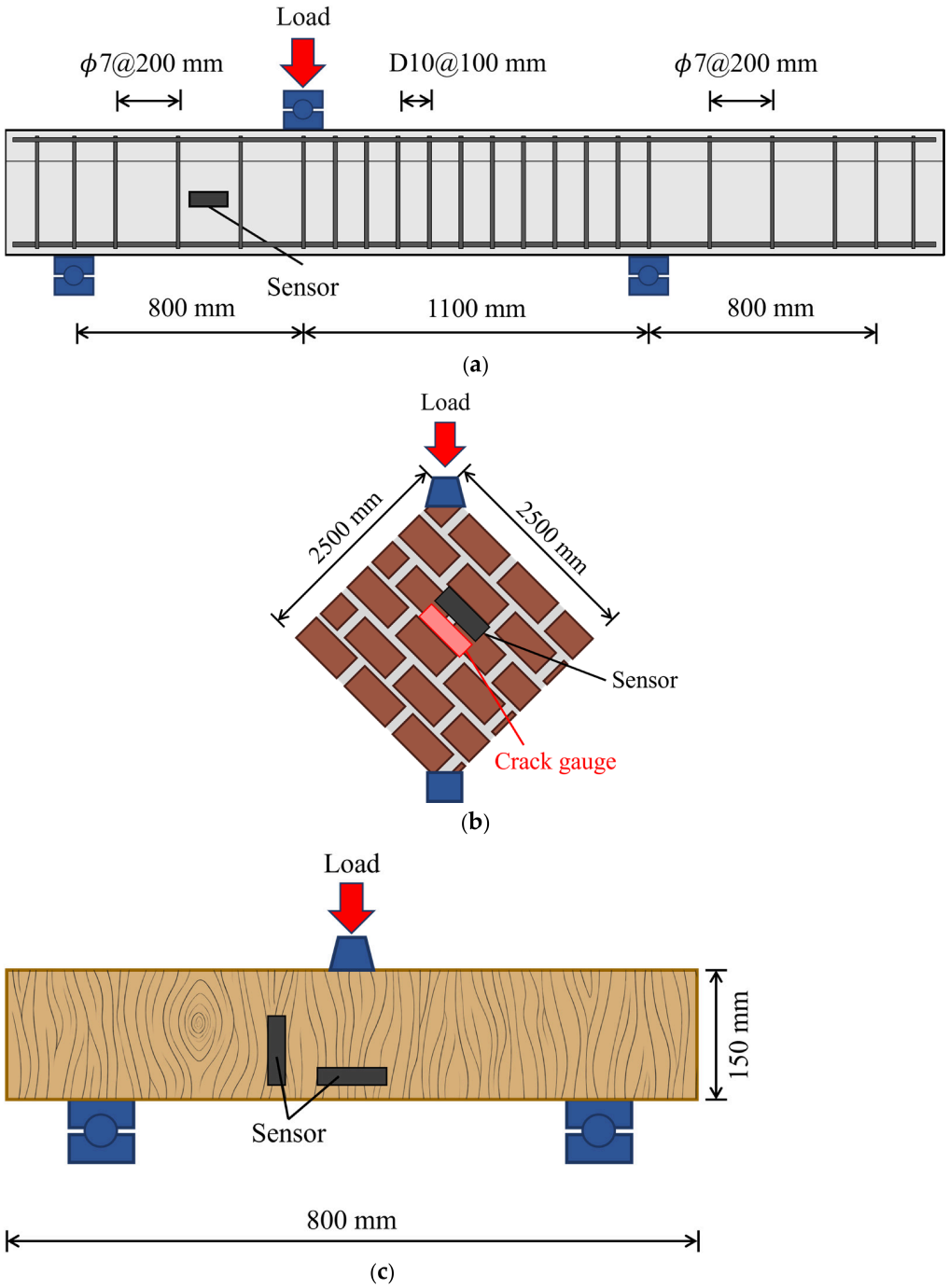


Figure 2. Test specimens and sensor measurement layout. (**a**) Concrete T-girder; (**b**) masonry wall; (**c**) timber beam and sensor placement.

The stirrups of the concrete girder consisted of $\phi 7$ bars at 200 mm spacing within the 850 mm test regions on both sides and D10 bars at 100 mm spacing within the central 1100 mm region. D25 bars were used as longitudinal tensile reinforcement, and D16 and

D10 bars were used as flange compression reinforcement. The material properties of the concrete and reinforcement are listed in Table 4. The sensor was attached at the location of an initial shear crack that formed at a low load stage. Sensor color and attachment condition were then observed during subsequent crack development. Crack width near the sensor was checked using a crack ruler during the test, and sensor color change and crack development were examined from the acquired images.

Table 3. Geometry and observation targets of the main specimens.

Specimen	Main Dimensions (mm)	Configuration and Observation Target
Concrete T-girder	Length 3000, overall height 400, top width 500, web width 200, flange thickness 100	Color change and attachment condition at the initial shear crack location
Masonry wall	Width 2500, height 2500	Crack development around mortar joints and adjacent bricks
Timber beam	Width 150, height 150, length 800	Crack development and sensor behavior during fracture

Table 4. Material properties of concrete and reinforcing bars.

Concrete	Reinforcing Bars							
	D25		D16		D10		ϕ7	
f_{ck} (MPa)	f_y (MPa)	E_s (GPa)	f_y (MPa)	E_s (GPa)	f_y (MPa)	E_s (GPa)	f_y (MPa)	E_s (GPa)
41	411	183.5	457	187.5	476	202.2	472	222.9

The masonry walls were tested in a wall shear configuration to induce cracking along the mortar joints between the loading and support regions. Preliminary tests were conducted to identify the locations of cracks developing along the mortar joints, and the sensor locations were selected based on these observations. The sensors were then placed across mortar joints near the loading and support regions, with the attachment regions positioned on adjacent brick surfaces. Crack gauges were installed near the sensor locations to observe crack behavior simultaneously. The effect of the surface step at the mortar joints on attachment stability was also examined. In addition, the attachment condition on the brick surfaces and the area available for crack observation were examined.

For the timber beam, sensor color change was observed during crack development and fracture in the bending test. The sensor was installed using a frame at the expected crack region near the center of the specimen. Separately, uniaxial tensile specimens were fabricated in a dog-bone shape with an overall length of 300 mm, a thickness of 25 mm, and a central width of 75 mm. Notches with a depth of 12.5 mm were introduced on both sides of the central region. In the uniaxial tensile tests, the target crack width was 1 mm, and the applied displacement was increased in 0.1 mm increments. Sensor color change associated with crack opening was recorded at each displacement increment. Because the crack paths were irregular, crack development and sensor color change were examined in the sensor installation region.

Table 5 summarizes the recorded conditions of five preliminary imaging and tensile trials conducted with different viewing angles, imaging distances, and illuminances. Initial trials used a 40° viewing angle at a 322 mm distance. Subsequent trials used 40° or 55° viewing angles at distances of 75–85 mm. The camera, sensor, and light source were positioned relative to one another using the fixed jig.

Table 6 summarizes the imaging conditions and measurement-device settings. The camera specifications provided in the experimental records were Samsung Galaxy S23, 8K video (7680 × 4320 pixels) at 30 fps, an F1.8 aperture, and automatic exposure and

ISO settings. The close-range imaging conditions and separate light source configuration adopted in the previous uniaxial calibration study [19] were used as references for the measurement device design. In this study, a jig and light-shielding housing were fabricated to maintain the relative positions of the sensor, camera, and light source. The imaging distance between the sensor and camera was fixed at 75 mm, the viewing angle was maintained between 40° and 50°, and the light source angle was fixed at 40°.

Table 5. Preliminary imaging and tensile-trial conditions reported in the experimental records.

Trial	Viewing Angle (°)	Distance (mm)	Illuminance (lx)
1	40	322	4561
2	40	322	2750
3	40	85	18,941
4	55	75	9847
5	55	80	4682/1539/3834

Table 6. Camera specifications and imaging conditions for the timber direct-tension test, measurement device, and previous calibration study.

Configuration	Parameter	Setting
Camera specifications in the experimental records	Model	Samsung Galaxy S23
Camera specifications in the experimental records	Video; aperture; exposure and ISO	7680 × 4320 pixels; 30 fps; F1.8; automatic
Timber direct-tension test	Imaging distance; viewing angle	75 mm; 40–55°
Timber direct-tension test	Image-acquisition step	0.1 mm displacement increment with a 4 s hold
Measurement device	Imaging distance; viewing angle	75 mm; 40–50° (design range)
Measurement device	Light-incidence angle	40° (fixed)
Measurement device	Ambient-light-shielding	Light-shielding acrylic housing
Previous uniaxial calibration [19]	Imaging distance; viewing angle	80 mm; 0°
Previous uniaxial calibration [19]	Light-incidence angle; illuminance	55°; 9847 lx

The previous uniaxial calibration study [19] used an 80 mm imaging distance, a 0° viewing angle, a 55° light-incidence angle, and an illuminance of 9847 lx. These reference conditions are reported separately from the timber direct-tension conditions and present measurement-device settings. A viewing-angle range of 40° to 50° was specified for the measurement device.

The housing and fixed jig shown in Figure 3 were designed to shield ambient light and maintain the relative positions of the camera, sensor, and light source. The housing and sensor holder were kept clear of the free sensing region and aligned during installation to avoid introducing initial deformation into the sensor. This configuration was used to maintain consistent imaging conditions during repeated measurements.

The proposed remote monitoring system combined the measurement device shown in Figure 3 with Long-Term Evolution (LTE) communication and an independent power supply. For sites where continuous external power is not readily available, a solar power supply configuration is proposed in Section 3.2.

A separate preliminary outdoor observation was carried out on a concrete specimen containing an existing crack. The sensor ends were fixed across the crack, and its condition was observed with a camera over approximately two months. This observation addressed attachment stability, image acquisition, and visible color changes.

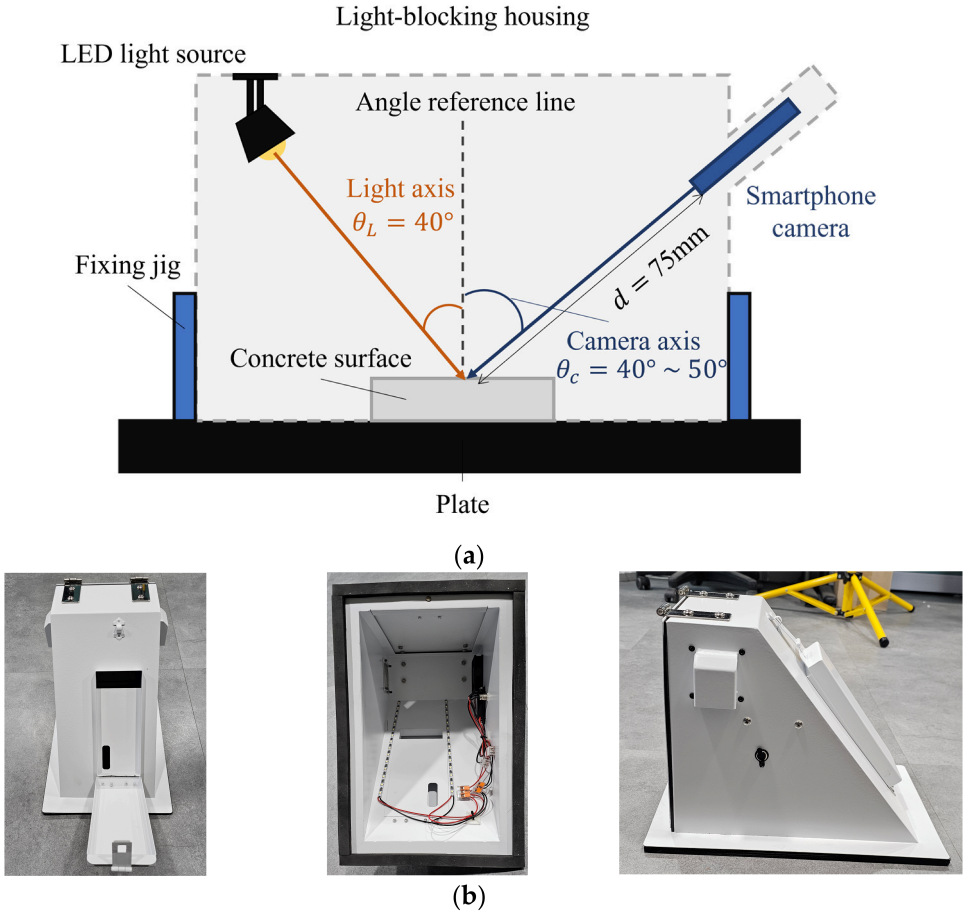


Figure 3. Measurement device for maintaining consistent imaging conditions. (**a**) Fixed jig for camera and light source positioning; (**b**) light-shielding housing and sensor observation region.

Images acquired at different test stages were used to qualitatively examine crack development, sensor attachment, and whether the sensor remained visible during cracking. Sensor color changes associated with crack development were also examined for concrete and timber. Color changes were examined qualitatively by comparing sensor images acquired at different stages under the recorded imaging conditions. When sensor detachment occurred during member failure, the corresponding crack and sensor attachment conditions were recorded.

3. Results

3.1. Sensor Attachment and Color Change in Different Materials

On the concrete surface, both ends of the sensor were fixed by adhesive bonding. Because the uncured adhesive could spread into the free sensing region, the sensor was kept horizontal after bonding. Adhesive flow was also checked during curing to limit intrusion into the free sensing region.

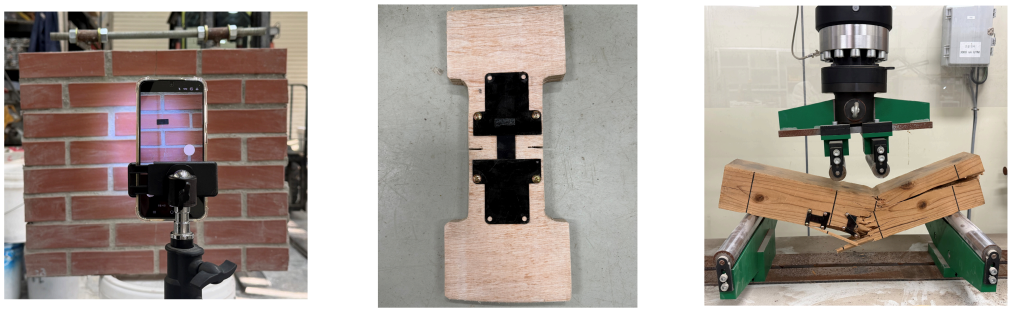
Figure 4 shows crack development, sensor color change, and attachment condition at different load stages of the concrete girder. The sensor installed at the initial shear crack exhibited a blue hue during the early load increase after sensor attachment and tended to change toward green as subsequent crack development was observed. At the shear failure stage, further crack development and sensor detachment from the concrete surface were observed.



(**a**) (**b**) (**c**)

Figure 4. Crack development, sensor color change, and attachment condition in the concrete girder. (**a**) Early loading after sensor attachment; (**b**) subsequent crack development stage; (**c**) shear failure and sensor detachment.

Figure 5 shows sensor installation and crack development for the masonry wall and timber specimens. For the masonry wall, direct bonding to the mortar joint could reduce attachment stability because of the surface step and different surface conditions of the brick and mortar. Accordingly, the sensor was attached to the adjacent brick surfaces to examine sensor attachment and crack observation. As shown in Figure 5a, the sensor and crack gauge were installed together, and images including both devices were acquired during crack development.



(**a**) (**b**) (**c**)

Figure 5. Sensor installation and crack development in masonry and timber specimens. (**a**) Sensor and crack gauge arrangement on the masonry wall; (**b**) frame-based sensor clamping for the timber uniaxial tensile test; (**c**) crack development and fracture of the timber beam.

In the timber uniaxial tensile tests, crack locations and directions varied among specimens. Crack width did not vary consistently with the applied displacement, which limited direct comparison of sensor color change at the same displacement level. As shown in Figure 5b, surface roughness, locally raised wood fibers, and debris and resin generated during testing could result in unstable sensor attachment conditions. The sensor was therefore secured with a light-shielding frame and positioned over the central region of the specimen to restrain displacement and rotation during testing.

As shown in Figure 5c, crack development was influenced by the grain direction, but the crack paths varied locally as the load increased. Sensor color change was observed during fracture. Because of the irregular crack paths, the corresponding color change could not be identified consistently. Sensors were placed in transverse and longitudinal directions because the crack location could not be identified in advance. Clear color changes were not consistently observed.

3.2. Application Considerations and Measurement Device

Application of the sensor to different structural materials requires consideration of material-specific surface and crack characteristics as well as consistent imaging conditions. Table 7 summarizes the main sensor observations and application considerations for concrete, masonry, and timber. In concrete, sensor detachment was observed at the shear failure stage. For masonry, the sensor location and attachment method were selected considering the surface step at the mortar joint and the different surface conditions of the brick and mortar. For timber, surface roughness and locally raised wood fibers could result in unstable sensor attachment conditions. Irregular crack paths also limited consistent comparison of sensor color changes.

Table 7. Main observations and application considerations for each material.

Target	Main Observation	Application Considerations
Concrete girder	Color change from blue toward green during crack development and sensor detachment at the shear failure stage	Sensor attachment stability and visual observation near the failure stage
Masonry wall	Sensor and crack gauge installation across the mortar joint with crack development recorded during loading	Surface step at the mortar joint and different surface conditions of brick and mortar
Timber	Irregular crack paths and limited identification of sensor color change during fracture	Irregular crack development and unstable direct attachment

The measurement device was fabricated using a fixed jig and a light-shielding housing to maintain the relative positions of the sensor, light source, and smartphone camera. The camera and light source were fixed at prescribed positions to maintain consistent imaging conditions during repeated image acquisition.

Figure 6 shows the conceptual image acquisition, communication, and power supply configuration for remote monitoring. In the proposed configuration, sensor images acquired by the smartphone would be transmitted through an LTE router and stored on a remote server. Power generated by the solar panel would be stored in a battery through a maximum power point tracking (MPPT) controller and supplied to the light-emitting diode (LED) light source, smartphone, and LTE router through a direct current-to-direct current (DC–DC) converter. The mechanochromic sensor requires no electrical power for structural color generation. Therefore, electrical power is required only for illumination, image acquisition, and data transmission. The proposed configuration is intended for sites where continuous external power is unavailable.

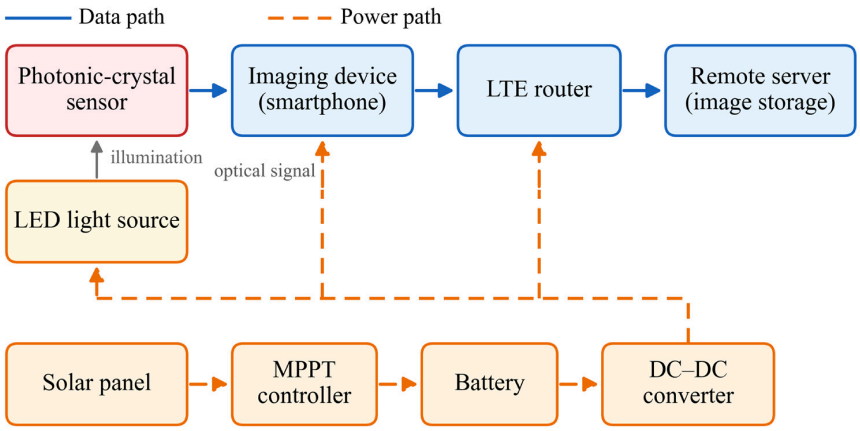


Figure 6. Conceptual image-acquisition, communication, and power-supply architecture for remote monitoring.

An initial remote image-acquisition setup enabled camera control, image capture, storage on the smartphone, and transfer to a researcher's PC through remote access. These functions are distinguished from the integrated LTE, remote-server, and solar-power architecture proposed in Figure 6.

Figure 7 shows the preliminary outdoor setup and sensor attachment on the pre-cracked concrete specimen. During the approximately two-month observation period, gradual structural-color changes and shortening or other changes in sensor shape were observed. Natural-light conditions also varied with time and weather.



(**a**) (**b**)

Figure 7. Preliminary outdoor observation setup and sensor attachment on a pre-cracked concrete specimen. (**a**) Outdoor observation setup; (**b**) attachment across the existing crack.

4. Discussion

4.1. Crack Deformation and Sensor Deformation Transfer

The color change of a mechanochromic sensor reflects the deformation transferred to the sensor across a crack. In structural components, the deformation transferred to the sensor depends on the relative displacement across the crack, sensor orientation, effective gauge length, and slip at the attachment regions. Let the effective gauge length between the two attachment regions be L_g and the change in sensor length within this region be $\Delta\ell_s$. The average sensor strain is defined by Equation (2). For a given change in sensor length, the average sensor strain depends on the effective gauge length. Slip at the attachment regions can also reduce the deformation transferred to the sensor.

$$\varepsilon_s = \frac{\Delta\ell_s}{L_g} \tag{2}$$

For a sensor crossing a single crack, the change in sensor length can be expressed in terms of crack opening and tangential slip under small deformation conditions. Neglecting continuous deformation of the surrounding material and out-of-plane deformation, the conceptual geometric approximation is expressed as follows:

$$\Delta\ell_s \approx \Delta w \cos\phi + \Delta s \sin\phi - \delta_{slip} \tag{3}$$

where Δw and Δs are the increments in crack opening normal to the crack and tangential slip, respectively, relative to the installation baseline. ϕ is the angle between the sensor longitudinal direction and the crack normal. δ_{slip} is the axial displacement not transferred to the sensor because of slip at the attachment regions. According to Equation (3), the change in sensor length depends on crack opening, tangential slip, sensor orientation relative to the crack, and attachment slip. When crack movement consists only of opening, the sensor is aligned

with the crack normal, and no attachment slip occurs, $\Delta\ell_s$ approaches Δw. Hoult et al. [5] separately measured crack opening and slip using DIC. Bassil et al. [3] and Zhang et al. [4] showed that interface behavior affects strain transfer at displacement discontinuities.

The amount of deformation transferred to the sensor also depends on material-specific attachment conditions. In concrete, large deformation near member failure can lead to sensor detachment. In masonry, surface steps and differences in surface condition across mortar joints can affect sensor placement and attachment. In timber, surface irregularities and variable crack paths can make stable direct attachment difficult. In this study, these effects were observed as sensor detachment at the shear failure stage of the concrete girder, adjustment of the sensor location and attachment method at the masonry joint, and unstable attachment conditions in timber.

For the same change in sensor length $\Delta\ell_s$, the average sensor strain decreases as the effective gauge length L_g increases. The effective gauge length therefore needs to be considered together with the attachment length and total sensor length. Sensor installation requires stable attachment at both ends while allowing the free sensing region to deform. For masonry with a surface step at the joint or timber with frame clamping, the attachment configuration can also affect deformation transfer to the sensor.

For a sensor installed across a pre-existing crack, the initial crack width w_0 and sensor image at the time of installation provide the baseline for subsequent observations. Crack development and sensor color change can then be compared with this initial state.

The installation baseline is distinguished from subsequent loading. In the concrete girder test, the sensor was attached at an initial shear crack formed at a low load stage, and subsequent color observations began after attachment.

4.2. Imaging Conditions and Measurement Considerations

The structural color of a photonic crystal-based sensor is affected by sensor deformation, lighting conditions, and observation geometry [14,19]. Consistent measurements at the same location therefore require maintaining the relative positions of the sensor, camera, and light source. In this study, the measurement device was designed to maintain these positions during image acquisition.

In the concrete girder test, the sensor detached at the shear failure stage, and further sensor color observation could not be performed. Therefore, sensor position and attachment condition should be confirmed before relating sensor color changes to crack deformation.

Movement or rotation of the sensor can change its position relative to the camera, and changes in the attachment condition can affect deformation transfer to the sensor. The camera support should remain mechanically independent of the sensor attachment region so that crack-induced displacement is not restrained. Potential interference between the measurement device and sensor should therefore be examined after installation.

Based on the component tests and use of the measurement device, Table 8 summarizes the main considerations for sensor installation and image acquisition. The initial sensor image, sensor location, attachment condition, and crack condition provide the baseline for subsequent observations.

Table 8. Main considerations for sensor installation and image acquisition.

Stage	Parameters and Conditions	Potential Issue
Target selection	Crack location and direction, crack width at installation	Uncertainty in the initial crack condition and observation location
Surface preparation	Surface flatness, surface step, contamination, and surface condition	Sensor lifting and unstable attachment

Table 8. *Cont.*

Stage	Parameters and Conditions	Potential Issue
Sensor attachment	Attachment length, effective gauge length, and sensing direction	Variation in deformation transfer and restraint of the free sensing region
Imaging conditions	Imaging distance, viewing angle, light source, focus, and exposure	Color variation caused by changes in imaging conditions
Initial recording	Initial sensor image, crack width, and sensor location	Uncertainty in the installation baseline
Repeated monitoring	Sensor detachment, rotation, contamination, communication status, and power status	Loss of sensor observation or measurement continuity

4.3. Application to Building Components

Application of the sensor to different building materials requires consideration of the attachment surface, crack location, and observation conditions. The attachment and measurement methods examined in this study primarily apply to surface cracks that are accessible for sensor installation and image acquisition. For concrete and masonry, sensor placement should account for the surface condition and the location where the sensor crosses the crack. For timber, the grain direction, crack location, and arrangement of the attachment points should be considered together. When a pre-existing crack is identified, the sensor can be installed across the crack, and the initial crack condition and sensor image can be recorded as the baseline for subsequent observations.

The sensor and camera perform complementary functions. The sensor converts local deformation into structural color within a defined sensing region, while the camera records the optical response. The intended role of the sensor is to provide a localized color response for observation at the selected attachment region. Comparative accuracy or detection performance relative to camera-only methods was not established in this study and remains a subject for future research.

This study focused on sensor attachment and visual observation. In concrete, sensor color change was observed during crack development. In timber, irregular crack paths limited consistent comparison of sensor color changes.

Future research should evaluate quantitative crack-monitoring performance through repeated tests with recorded numbers of specimens and sensors, synchronized independent crack-width measurements, and analysis of sensor color changes in the acquired images. These tests should assess sensitivity, resolution, usable range, repeatability, and uncertainty, together with the effects of attachment conditions and camera and lighting settings. Controlled optical observations should support criteria for distinguishing crack-induced color changes from variations caused by imaging conditions. Future studies on early-age and time-dependent cracking should examine sensor installation before crack initiation and distinguish structural crack development from sensor drift and hysteresis under varying environmental and loading conditions. Validation of the proposed remote-monitoring architecture should address power autonomy, communication reliability, and long-term image stability.

5. Conclusions

This study applied a photonic crystal-based mechanochromic sensor to concrete, masonry, and timber components and examined sensor attachment and observation under different surface and crack conditions. The documented cases identified attachment and detachment in concrete, installation considerations around masonry joints, and frame-based positioning and irregular crack paths in timber. Based on these observations, considerations for sensor attachment and image acquisition were presented. A measurement device was

developed to maintain the relative positions of the sensor, camera, and light source. The main findings and application considerations are as follows.

1. Sensor attachment should be adapted to the surface condition of each material. For concrete, adhesive bonding at both ends was applied while maintaining a free sensing region. For masonry, attachment to adjacent brick surfaces was combined with mechanical clamping considering the surface step at the mortar joint and the different surface conditions of the brick and mortar. For timber, frame-based clamping was applied considering surface roughness and locally raised wood fibers.
2. In the concrete girder, the sensor tended to change from blue toward green as the crack developed, and sensor detachment was observed at the shear failure stage. For masonry, the sensor and crack gauge were installed around the mortar joints, and crack development was recorded during loading. In the timber beam, irregular crack paths limited clear identification of sensor color change during fracture.
3. The relationship between sensor color change and crack deformation depends on the deformation transferred to the sensor. The change in sensor length can be affected by crack opening, sensor orientation relative to the crack, tangential slip, and attachment slip. For the same change in sensor length, the average sensor strain also depends on the effective gauge length. The sensor attachment method should therefore be selected with consideration of deformation transfer. Equation (3) is a conceptual geometric approximation.
4. Consistent measurements at the same location require maintaining the relative positions of the sensor, camera, and light source. In this study, a measurement device using a fixed jig and light-shielding housing was developed to maintain these positions during image acquisition. Sensor position and attachment condition should also be confirmed before relating sensor color changes to crack deformation.
5. The attachment and image-acquisition procedures examined in this study primarily apply to surface cracks in building components that are accessible for sensor installation and image acquisition. For pre-existing cracks, the crack width and sensor image at the time of installation can be recorded as the baseline for observation of crack development after installation. In addition, a conceptual remote monitoring system integrating image acquisition, LTE communication, and a solar power supply was proposed for sites where continuous external power is unavailable. Preliminary outdoor observations showed gradual color and sensor-shape changes, and initial remote camera-control and image-transfer functions were implemented.

Author Contributions: Conceptualization, K.-C.K. and G.-S.R.; methodology, K.-C.K.; validation, Y.K. and C.K.; formal analysis, K.-C.K.; investigation, Y.K.; resources, G.-S.R.; data curation, G.-S.R.; writing—original draft preparation, C.K.; writing—review and editing, Y.K. and C.K.; visualization, Y.K.; supervision, C.K.; project administration, K.-C.K.; funding acquisition, K.-C.K. All authors have read and agreed to the published version of the manuscript.

Funding: This work was supported by the National Research Foundation of Korea (NRF) grant funded by the Korean government (MSIT) in 2023 (Grant No. RS-2023-00254093, Project Title: Development of Smart Monitoring System for Safety and Risk Management of Buildings based on Nanophotonics and Machine-Learning).

Data Availability Statement: The data presented in this study are available on request from the corresponding author.

Acknowledgments: During the preparation of this manuscript, the authors used Claude (Anthropic) for translation and language editing. The authors have reviewed and edited the output and take full responsibility for the content of this publication.

Conflicts of Interest: The authors declare no conflicts of interest.

References

1. Poursaee, A.; Ross, B. The Role of Cracks in Chloride-Induced Corrosion of Carbon Steel in Concrete—Review. *Corros. Mater. Degrad.* **2022**, *3*, 258–269. [CrossRef]
2. Yan, J.; Downey, A.; Cancelli, A.; Laflamme, S.; Chen, A.; Li, J.; Ubertini, F. Concrete Crack Detection and Monitoring Using a Capacitive Dense Sensor Array. *Sensors* **2019**, *19*, 1843. [CrossRef]
3. Bassil, A.; Chapeleau, X.; Leduc, D.; Abraham, O. Concrete Crack Monitoring Using a Novel Strain Transfer Model for Distributed Fiber Optics Sensors. *Sensors* **2020**, *20*, 2220. [CrossRef]
4. Zhang, S.; Liu, H.; Cheng, J.; DeJong, M.J. A mechanical model to interpret distributed fiber optic strain measurement at displacement discontinuities. *Struct. Health Monit.* **2021**, *20*, 2584–2603. [CrossRef]
5. Hoult, N.A.; Dutton, M.; Hoag, A.; Take, W.A. Measuring Crack Movement in Reinforced Concrete Using Digital Image Correlation: Overview and Application to Shear Slip Measurements. *Proc. IEEE* **2016**, *104*, 1561–1574. [CrossRef]
6. Cha, Y.-J.; Choi, W.; Büyüköztürk, O. Deep Learning-Based Crack Damage Detection Using Convolutional Neural Networks. *Comput.-Aided Civ. Infrastruct. Eng.* **2017**, *32*, 361–378. [CrossRef]
7. Belloni, V.; Sjölander, A.; Ravanelli, R.; Crespi, M.; Nascetti, A. Crack Monitoring from Motion (CMfM): Crack detection and measurement using cameras with non-fixed positions. *Autom. Constr.* **2023**, *156*, 105072. [CrossRef]
8. Omoniyi, T.M.; Abel, B.; Omoebamije, O.; Onimisi, Z.M.; Matos, J.C.; Tinoco, J.; Minh, T.Q. The Effect of Data Augmentation on Performance of Custom and Pre-Trained CNN Models for Crack Detection. *Appl. Sci.* **2025**, *15*, 12321. [CrossRef]
9. Ribeiro, D.; Rakoczy, A.M.; Cabral, R.; Hoskere, V.; Narazaki, Y.; Santos, R.; Tondo, G.; Gonzalez, L.; Matos, J.C.; Massao Futai, M.; et al. Methodologies for Remote Bridge Inspection—Review. *Sensors* **2025**, *25*, 5708. [CrossRef]
10. Bae, G.; Seo, M.; Lee, S.; Bae, D.; Lee, M. Colorimetric Detection of Mechanical Deformation in Metals using Thin-Film Mechanochromic Sensor. *Adv. Mater. Technol.* **2021**, *6*, 2100479. [CrossRef]
11. Bae, G.; Seo, M.; Lee, S.; Bae, D.; Lee, M. Angle-Insensitive Fabry–Perot Mechanochromic Sensor for Real-Time Structural Health Monitoring. *Adv. Mater. Technol.* **2021**, *6*, 2100118. [CrossRef]
12. Pyeon, S.-J.; Choe, G.-C.; Kim, H.-S.; Kim, G.-Y.; Nam, J.-S. An Experimental Study on the Applicability of Mechanochromic Sensors for Monitoring Tensile Strain of Concrete Materials. *J. Korea Inst. Build. Constr.* **2021**, *21*, 573–581. (In Korean) [CrossRef]
13. Pyeon, S.; Kim, H.; Choe, G.; Lee, M.; Jeon, J.; Kim, G.; Nam, J. Crack Evaluation of Concrete Using Mechanochromic Sensor. *Materials* **2023**, *16*, 662. [CrossRef]
14. Minh, N.H.; Kim, K.; Kang, D.H.; Yoo, Y.-E.; Yoon, J.S. An angle-compensating colorimetric strain sensor with wide working range and its fabrication method. *Sci. Rep.* **2022**, *12*, 21926. [CrossRef]
15. Quan, Y.-J.; Kim, Y.-G.; Kim, M.-S.; Min, S.-H.; Ahn, S.-H. Stretchable Biaxial and Shear Strain Sensors Using Diffractive Structural Colors. *ACS Nano* **2020**, *14*, 5392–5399. [CrossRef]
16. Hoang Minh, N.; Kim, K.; Kang, D.H.; Yoo, Y.-E.; Yoon, J.S. Photonic Crystals for Dichotomous Sensitivity to Strain for Sensor and Indicator Applications. *ACS Appl. Nano Mater.* **2024**, *7*, 20361–20369. [CrossRef]
17. Battisti, A.; Minei, P.; Pucci, A.; Bizzarri, R. Hue-based quantification of mechanochromism towards a cost-effective detection of mechanical strain in polymer systems. *Chem. Commun.* **2017**, *53*, 248–251. [CrossRef]
18. Kang, D.; Kim, Y.; Kim, C.; Lee, M. Highly Flexible Infrared Emitter with Spatially Controlled Emissivity for Optical Security. *Adv. Mater. Technol.* **2023**, *8*, 2200808. [CrossRef]
19. Choi, W.-J.; Yang, M.; You, I.; Yoon, Y.-S.; Ryu, G.-S.; An, G.-H.; Yoon, J.S. Discoloration Characteristics of Mechanochromic Sensors in RGB and HSV Color Spaces and Displacement Prediction. *Appl. Sci.* **2025**, *15*, 1066. [CrossRef]

Disclaimer/Publisher's Note: The statements, opinions and data contained in all publications are solely those of the individual author(s) and contributor(s) and not of MDPI and/or the editor(s). MDPI and/or the editor(s) disclaim responsibility for any injury to people or property resulting from any ideas, methods, instructions or products referred to in the content.